Toward understanding optical properties of amyloids: a reaction path and nonadiabatic dynamics study

Luca Grisanti,*,†,‡ Marin Sapunar,¶ Ali Hassanali,‡ and Nađa Došlić*,¶

†*Division of Theoretical Physics, Ruđer Bošković Institute, Bijenička cesta 54, 10000 Zagreb, Croatia*

‡*Condensed Matter and Statistical Physics, International Centre for Theoretical Physics, Strada Costiera 11, Trieste 34151 Italy*

¶*Division of Physical Chemistry, Ruđer Bošković Institute, Bijenička cesta 54, 10000 Zagreb, Croatia*

E-mail: lgrisant@irb.hr; nadja.doslic@irb.hr

Abstract

Amyloids have unique structural, chemical and optical properties. Although much theoretical effort has been directed toward understanding amyloid nucleation, the understanding of their optical properties has remained rather limited. In particular, the photophysical mechanisms leading to near UV excitation and characteristic blue-green luminescence in amyloid systems devoid of aromatic amino acids have not been resolved.

We use *ab initio* static calculations and nonadiabatic dynamics simulations to study the excited electronic states of model amyloid-like peptides. We show that their photophysics is essentially governed by the multitude of $n\pi^*$ states with excitation localized on the amide groups. The strong stabilization of the $n\pi^*$ states with respect to the amide group deplanarization and the concomitant increase of the oscillator strength makes excitation in the near UV possible. With respect to emission, our dynamics simulations revealed that the amyloid cross β arrangement effectively hinders the nonradiative relaxation channels usually operative in proteins. Finally, we show that after relaxation of the photoexcited peptides toward the minimum of the different $n\pi^*$ states, fluorescence takes place in the visible (green) part of the electromagnetic spectrum.

Introduction

Amyloids are self-assembled polypeptides characterized by a cross β arrangement in which highly ordered β-strands are interconnected by hydrogen bonds.[1–3] Owing to their association with a range of human diseases, numerous experimental and theoretical studies have focused on the mechanism of amyloid formation.[4–9] Considerable attention has also been devoted to their remarkable optical properties, rarely found in proteins.[10–13] An in–depth understanding of these properties is important for both fundamental and translational research, as it could help the development of diagnostic tools for probing and monitoring the formation of toxic fibrils.[14]

Under excitation at $380 - 340$ nm ($3.3 - 3.6$ eV), amyloids show luminescence in the $530 - 440$ nm ($2.3 - 2.8$ eV) range.[11–13,15,16] The photophysical mechanisms of both excitation at wavelengths above 250 nm and of blue-green luminescence, are still not resolved.[12,17–19] Particularly puzzling is the fact that the rather

weak blue-green luminescence has been observed also in amyloid systems without aromatic amino acids,[13,20,21] as well as in nanostructures and nanodots with amyloid-like structures.[22–24] Here, by focusing on small peptide systems mimicking amyloids , we disclose a possible mechanism underlying both the excitation and luminescence.

In the absence of aromatic amino acid residues, the UV-light absorbing groups in proteins are the amide groups constituting the peptide backbone, the terminal amino and carboxyl groups as well as the amino, amide and carboxyl groups present in the side chains of some amino acids. Each amide group gives rise to a weak and localized n$\rightarrow \pi^*$ transition at $\sim$ 5.5 eV and an intense $\pi \rightarrow \pi^*$ transition beyond $\sim$ 6.0 eV.[25–27] Transitions with nonlocal excitation where charge is translocated between amide groups in the protein backbone are predicted to be higher in energy.[27]

The emitting states in proteins are the $\pi\pi^*$ states localized on the side chains of the three aromatic amino acids: tryptophan (Trp), tyrosine (Tyr) and phenylalanine (Phe) with the main contribution arising from Trp (indole) emission at around 350 nm.[28] The low lying states of peptides and proteins devoid of chromophoric amino acids usually have access to efficient nonradiative relaxation mechanisms which makes them nonfluorescent. These mechanisms include electron driven proton transfer along hydrogen bonds in γ and β turns,[29–31] $\pi\sigma^*$ mediated dissociation[32–34] and large amplitude torsional deformations of the peptide backbone which efficiently quench fluorescence of the amide nπ^* states.[35,36] Conformer-specific studies on small peptides have shown, however, that the efficiency of the nonradiative decay depends sensitively on the peptide secondary structure, that is, on the local environment in which the photoexcited chromophore is embedded.[37] In the case of the capped dipeptide N-acetylphenylalaninylamide, for example, the β-strand conformer had a significantly longer excited state lifetime (70 ns) than the folded $\gamma(g+)$-conformer (1.5 ns).[35] Thus, the cross β-arrangement of amyloids is likely to hinder nonradiative relaxation by restricting the access to conical intersections with the electronic ground state.[38]

Altogether, a molecular-level explanation of the optical properties of amyloids requires the identification of the absorbing and emitting electronic states, as well as an assessment of structural and electronic factors that hinder the nonradiative decay. To this aim we have performed extensive *ab initio* static calculations and nonadiabatic dynamics simulations for a range of model β-strand peptides displaying intra- and inter-chain interactions characteristic for amyloid systems. We show that their peculiar optical properties arise from the multitude and strong coordinate dependence of the amide nπ^* states. More specifically, we show that the excitation energy of the n$\rightarrow \pi^*$ transitions strongly decreases upon deplanarization of the amide group on which they are localized to the extent that each of these transitions may become stabilized as the lowest one in energy and emit in the visible range of the electromagnetic spectrum.

Results

Figure 1 shows three computationally-accessible model peptides obtained starting from the amyloidic sequence Aβ_{30-35}[39] and displaying the characteristic hydrogen bonding pattern of parallel β-strands (see Supporting Information for details). Systems **2B7** and **2B11** contain respectively 7 and 11 carbonyl groups, while **3B11** encompasses 3 β-strands and 11 carbonyl groups. To both lower the computational costs and focus attention on the intrinsic characteristics of the amide backbone, glycine is adopted as the amino acidic unit.

Excitation mechanism

For all model systems we run unconstrained *ab initio* Born-Oppenheimer molecular dynamics simulations at the DFT level.[40–42] Then, by collecting a series of frames from the ground state dynamics we investigated the structure of the excited electronic states in the Franck-Condon region using the ADC(2) method.[43,44] For fur-

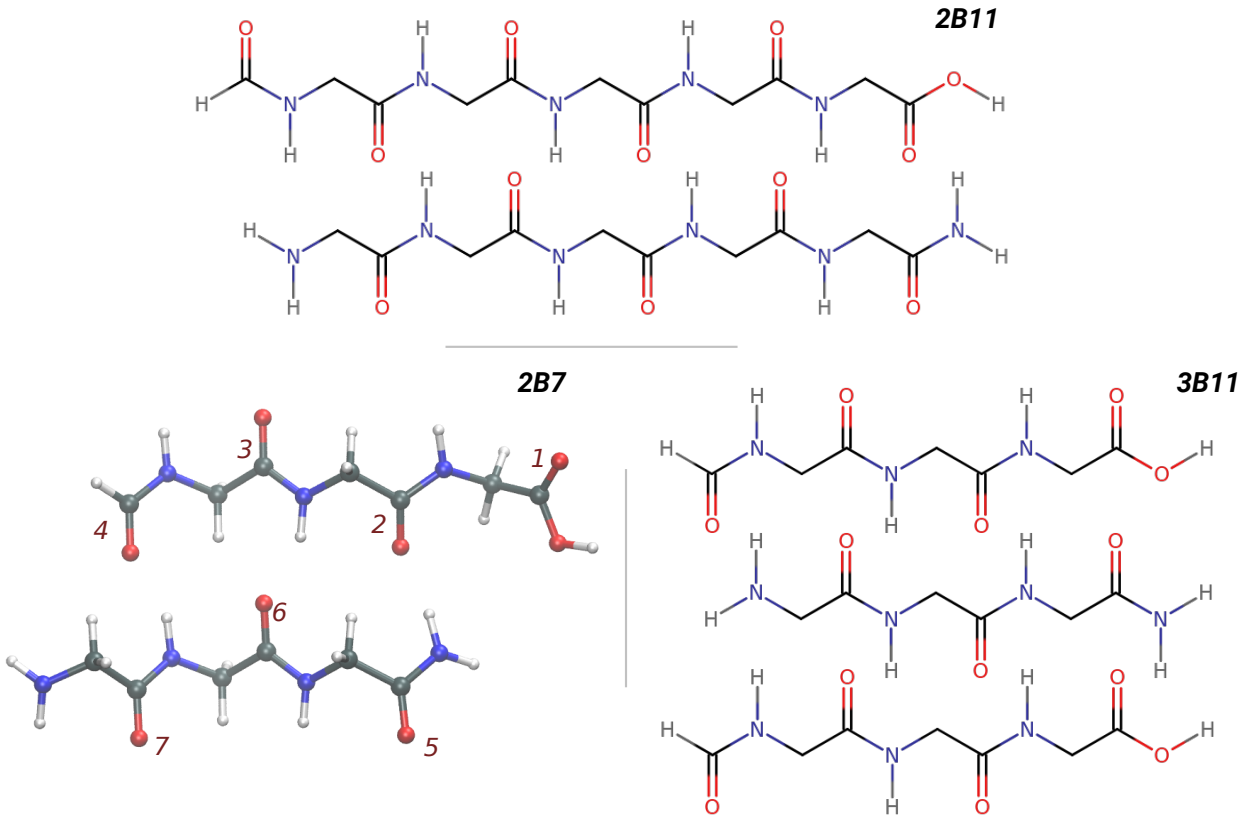

Figure 1: Structure of the investigated model systems, exhibiting double (**2B7** and **2B11**) and triple (**3B11**) β-strand structures. The numeration of carbonyl groups is given for **2B7**, represented as 3D model in its reference structure 2B7(C). For the Cartesian coordinates see the Supporting Information.

ther details see the Computational Methods and Supporting Information. The computed density of electronic states (Figure S1) and the absorption spectra (Figure S2) show that, for all systems, the first group of states lying between 4.5 and $\sim$ 6 eV is of nπ^* character and carries low oscillator strength, while the second group is markedly bright and includes both localized ($\pi\pi^*$) and charge transfer states.[25–27] This suggests that the experimental 3.3$-$3.6 eV excitation window corresponds to the low energy tail of the absorption spectrum with very low intensity.

Thus, to unravel the excitation mechanism one would need to search for "rare" geometries in the ground state distribution which are likely candidates for excitation. Here we opted for a different approach and begin by exploring the topography of the low lying excited states using nonadiabatic dynamics simulations. These simulations will provide information on the nuclear motion in the Franck-Condon region and help identify the structural characteristics of the "rare" geometries we are interested in.

For the two larger systems **2B11** and **3B11** that best capture the amyloid structure we run several short (10 $-$ 15 fs) nonadiabatic dynamics trajectories starting from structures sampled ground state dynamics vertically excited to the nπ^* manifold. Figure 2 shows the time dependence of the potential energy of the lowest 20 electronic states along a **2B11** trajectory. One can see that two electronic states are stabilized, meaning that their potential energy decreases during the dynamics, while the energy of all other states increases. These are the initially excited (populated) S_2(nπ^*) state (line with blue dots) and a higher lying $\pi\pi^*$ state which begins as S_{19} at $t = 0$ and becomes S_2 (orange line) at $t = 5.5$ fs. The electronic

excitation of both stabilized states is localized on the same carbonyl unit (see panel c). **3B11** shows a very similar dynamical behaviour (Figure S3, also insets of S7 and S8). The energy stabilization of the two pairing states is very large. In **2B11**, the initially populated $S_2(n\pi^*)$ drops by 1.5 eV in only 6 fs, while the pairing $\pi\pi^*$ state, initially above 6.5 eV descends below 5.8 eV. This large decrease of the potential energy of the initially excited $n\pi^*$ state is caused by motion towards the minimum of this state which in terms of structural changes includes a deplanarization of the amide group on which the excitation is localized, and elongation of the corresponding C=O bond.

The picture emerging from the dynamics simulations is that $n\rightarrow\ \pi^*$ transitions at deplanarized amide geometries might be the ones susceptible to near UV excitation. Since all $n\pi^*$ states are highly localized, we assume that the general properties of these states are similar in all systems and turn to the more tractable system **2B7**. Vertical excitation energies of the lowest 7 electronic states of a reference **2B7** structure, denoted **2B7(C)**, are shown in Table 1. All states are of $n\pi^*$ character with excitation localized on the carboxyl ($n_1\pi_1^*$) and the 6 amide groups (for numeration, see Figure 1) and are found $5.17 - 5.46$ eV above the ground state, while the oscillator strengths range between 6×10^{-4} and 1.2×10^{-3}. A πRyd state with excitation localized on the terminal amino group is found at 6.29 eV, while the $\pi\pi^*$ manifold starts above 6.54 eV. We note that at the SCS-ADC(2)/aug-cc-pVDZ level the πRyd state is significantly redshifted and found at 4.94 eV, while the $n\pi^*$ states remained almost unchanged (see Table S1). Optimizations of each of the 7 $n\pi^*$ states were then performed. To avoid formation of more stable γ-turns,[45] only the region around the corresponding amide group was allowed to relax, meaning that the obtained values are upper bounds of adiabatic excitation energies (see Supporting Information). The adiabatic excitation energies are collected in Table 2 while the most important structural parameters: the deplanarization angles $\theta_N(\mathrm{H}_i\ \mathrm{C}_i^\alpha\ \mathrm{C}_{i-1}\ \mathrm{N}_i)$ and $\theta_C(\ \mathrm{N}_{i+1}\ \mathrm{C}_i^\alpha\ \mathrm{O}_i\ \mathrm{C}_i)$ of the amide group on which the excitation is localized and the corresponding C=O bond distance are given in Table S2. Compared to vertical excitation energies, adiabatic excitations are redshifted by $\approx$ 1.4 eV, while each of the 7 $n\pi^*$ states becomes S_1 at its minimum. The SCS-ADC(2)/aug-cc-pVDZ optimization of the πRyd state resulted in an adiabatic excitation energy of 4.68 eV meaning that the state remains far above the $n\pi^*$ minima (see Table S3).

While adiabatic excitation energies fall well within the experimental excitation window the significant difference of the amide group geometry between the reference ground state structure and the corresponding $n\pi^*$ minimum indicates that resonant adiabatic excitation should be inefficient, if possible at all. This can also be inferred from the significant rise in the energy of S_0 at the different $S_1^{min}(n\pi^*)$ minima (see Tables 2 and S3).

To locate a possible excitation region, we take a closer look at the topography of the $n\pi^*$ states in relation with the electronic ground state and analyze the energy profiles from the Franck-Condon geometry to the $n\pi^*$ minima in terms of the two key motions: the deplanarization of the amide group and C=O bond stretching. Figures 3 and S4 show that the two motions affect the ground and excited states in different ways. The $n\pi^*$ potential is relatively flat with respect to C=O stretching, but the energy of the ground state increases steeply on the way to the $n\pi^*$ minimum. On the other hand, the deplanarization of the peptide bond only weakly destabilizes the ground state, but strongly stabilizes the $n\pi^*$ states. In addition, the out-of-plane deformation increases the $n\pi^*$ oscillator strength by an order of magnitude. This would make nonplanar amide and carboxyl groups likely candidates for near UV absorption. However, peptide structures in which the ground state is not destabilized by C=O bond elongation are also promising candidates. The latter happens when a C=O bond is engaged in a strong hydrogen bond interaction. A prediction for the statistical relevance of the former is more difficult and it is also a subject of biochemical interest[46] because of the enhanced reactivity of distorted amide groups. While molecular modeling has shown that the distor-

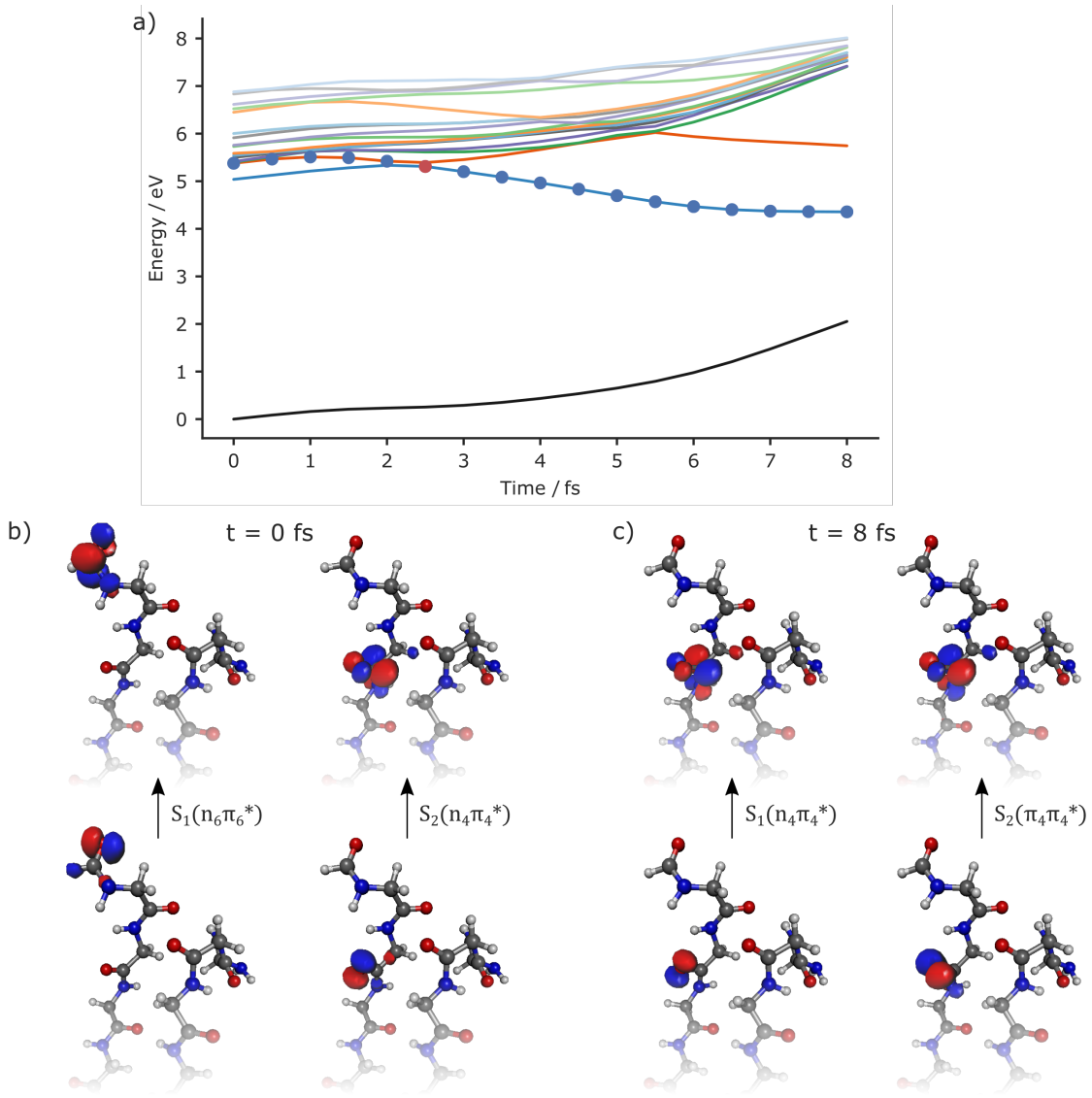

Figure 2: (a) Time dependence of the potential energies of the electronic ground state (black) and the lowest 20 adiabatic electronic states of **2B11** along a selected nonadiabatic trajectory computed at the ADC(2)/cc-pVDZ level. Blue circles denote the currently populated electronic state. (b, c) Partial view of the molecule at the beginning (b) and end (c) of the trajectory showing the hole (bottom) and particle (top) NTOs describing the excitation to the two lowest excited states. The potential energy of the photoexcited $n\pi^*$ state (initially S_2, blue dots) and the bright $\pi\pi^*$ state (initially S_{19} and S_2 after 6 fs) with excitation localized at the same amide group decreases during the dynamics, while the energy of the other states increases. The orbital indices correspond to the numeration of the carbonyl groups where 1 is assigned to COOH.

tion of an amide group from its planar configuration is supported by β-sheet hydrogen bonding,[47] we can only say that the high density of $n\pi^*$ states in amyloids certainly increases the probability of excitation.

Excited state dynamics and fluorescence

Having established an excitation mechanism, we move to examining whether the β-strand

Table 1: Spectral assignment, vertical excitation energies (in eV) and oscillator strengths (f_{osc}) of the lowest 7 nπ^* transitions computed at the reference ground state geometry of **2B7(C)**. Excitations are localized on the 6 amide groups and the terminal carboxyl group. For the numeration of the groups see Figure 1. Calculations were performed at the ADC(2)/cc-pVDZ level.

State	S_1 ($n_5\pi_5^*$)	S_2 ($n_7\pi_7^*$)	S_3 ($n_1\pi_1^*$)	S_4 ($n_3\pi_3^*$)	S_5 ($n_2\pi_2^*$)	S_6 ($n_6\pi_6^*$)	S_7 ($n_4\pi_4^*$)
E	5.18	5.27	5.31	5.34	5.43	5.46	5.46
f_{osc}	0.0012	0.0008	0.0011	0.0022	0.0007	0.0043	0.0006

Table 2: Adiabatic excitation energies (in eV) of the 7 nπ^* states of **2B7** computed at the partially optimized geometry for each state (S_1^{min}). Energies of the electronic ground state (S_0) and second excited state (S_2, the pairing $\pi\pi^*$ state) are also given with respect to the **2B7(C)** ground state energy. Oscillator strengths are given in parenthesis. Calculations were performed at the ADC(2)/cc-pVDZ level.

State	$n_1\pi_1^*$	$n_2\pi_2^*$	$n_3\pi_3^*$	$n_4\pi_4^*$	$n_5\pi_5^*$	$n_6\pi_6^*$	$n_7\pi_7^{*a}$
S_0	1.96	1.97	1.94	2.61	1.80	2.12	1.50
S_1^{min}(nπ^*)	3.82	4.01	4.07	4.48	3.75	4.09	3.43
	(0.0009)	(0.0005)	(0.0011)	(0.0008)	(0.0009)	(0.0005)	(0.0014)
$S_2(\pi\pi^*)$	6.09	5.44	5.65	6.18	5.72	5.49	5.18
	(0.0704)	(0.0905)	(0.0900)	(0.1225)	(0.0966)	(0.0900)	(0.0843)

[a] Full optimization of the state was achieved.

structure of amyloids prevents efficient nonradiative relaxation. This is known to be the case for single β-strand peptides[37] but alternative deactivation channels, such as an electron driven H-transfer between β-strands, might be operative in amyloids. To unravel possible relaxation mechanisms we performed nonadiabatic dynamics simulations for **2B7**. Initial geometries and velocities were sampled from the ground state MD simulations and all trajectories, 15 with parallel and 6 with anti-parallel β-strand arrangement, were vertically excited to the nπ^* manifold (S_1-S_5). Thus, compared to the experimental excitation we imparted $\approx$ 1 eV more energy to the system allowing it to explore a larger region of the potential energy surface. Within the first $10-15$ fs of the dynamics, all trajectories reached the S_1 state. This fast stabilization to the S_1 state is analogous to the one observed in the short **2B11** (Figure 2) and **3B11** (Figure S3) trajectories. Despite the fast relaxation to S_1 only 1/3 of trajectories deactivated to the ground state by the end of our 250 fs long simulations. As expected, we found that most of the trajectories that returned to the ground state deactivated by torsion of the terminal amide group. However, the description of the terminal groups in our model does not accurately represent the situation in amyloids where we expect such torsions to play a less prominent role.

To simulate the fluorescence spectrum of **2B7** we computed vertical emission energies and $S_1 \rightarrow S_0$ transition dipole moments along nonadiabatic trajectories and averaged over three time intervals.[48] The upper panels of Figure 4 show the dependence of the oscillator strength of the currently populated electronic state on the length of the excited C=O bond (left) and the corresponding torsional angle θ_C (right). The latter increases the oscillator strength of the populated nπ^* to the 10^{-2}-10^{-1} range, while

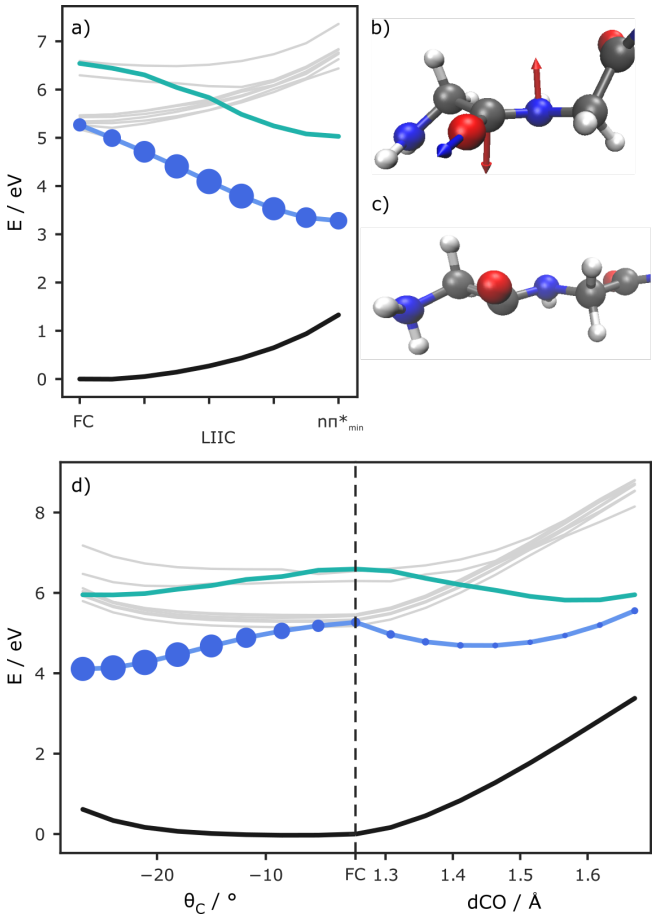

Figure 3: Upper panels: Relative ADC(2)/cc-pVDZ energies (in eV) of the ground (black), $n_7\pi_7^*$ (blue), $\pi_7\pi_7^*$ (green) and other 8 excited states (grey) of **2B7** along the linearly interpolated path (LIP) from the reference Franck-Condon geometry to the $n_7\pi_7^*$ state minimum (a). Fragment of **2B7** showing the photoexcited amide group (b and c). The arrows indicate the structural changes encompassed in the LIP. Lower panel: The effects of decoupling the deplanarization of the peptide bond (θ_N and θ_C) from the $(C{=}O)_7$ stretching motion are shown on the left and right panel, respectively. The oscillator strengths of the $n_7\pi_7^*$ state is indicated by blue circles of different areas.(d)

the former has an opposite effect. These non-negligible oscillator strengths sampled during the dynamics clearly indicate that fluorescence from the $S_1(n\pi^*)$ state should be possible.

The time evolution of the computed fluorescence spectrum is shown in the lower panel of Figure 4. In the first interval, from 15 to 40 fs, the spectrum is peaked at 3.3 eV. During this time all trajectories reached the S_1 state, but intramolecular vibrational redistribution could not be completed. The subsequent redshift of the emission spectrum down to 2.0 eV (620 nm) in the $40-100$ and $100-235$ fs time windows reflects the relaxation of **2B7** on the S_1 state. Because of the rather short time propagation and excess energy in the initial conditions, we consider the computed spectrum only as an estimate of the fluorescence spectrum. However, the accuracy of the calculations can be assessed by comparing the center of the fluorescence spectrum obtained from dynamics simulations to its static counterpart, that is, the average vertical emission energy, $\Delta E = E(S_1^{min}) - E(S_0)$, of 1.99 eV computed at the minima of the $n\pi^*$ states (see Table 2). Clearly, in both static and dynamics computations the emission is peaked in the visible meaning that despite its apparent simplicity, our **2B7** model system captures well the blue-green fluorescence ($2.3-2.7$ eV) observed in several different experiments.[11–13,15,16]

Discussion

In this work we propose a photophysical mechanism that could be the base of the near UV excitation and blue-green luminescence observed in amyloid systems. Excitation in the near UV is possible at geometries with a deplanarized amide group at which a slight destabilization of the ground state is accompanied by a significant stabilization of the corresponding $n\pi^*$ state ($>$ 1.0 eV) and increase of its oscillator strength. With respect to the emission we found that after excitation to an $n\pi^*$ state the system evolves toward the minimum which in addition to the deplanarization of the amide group is also characterized by an extended carbonyl bond. As a stretched carbonyl unit is strongly destabilizing for the ground state the emission from the minimum of the $n\pi^*$ state is shifted to the visible.

To draw a comprehensive photophysical picture of the observed blue-green luminescence we consider previously reported results and compare them to our results. The overall perception is that hydrogen bonding interac-

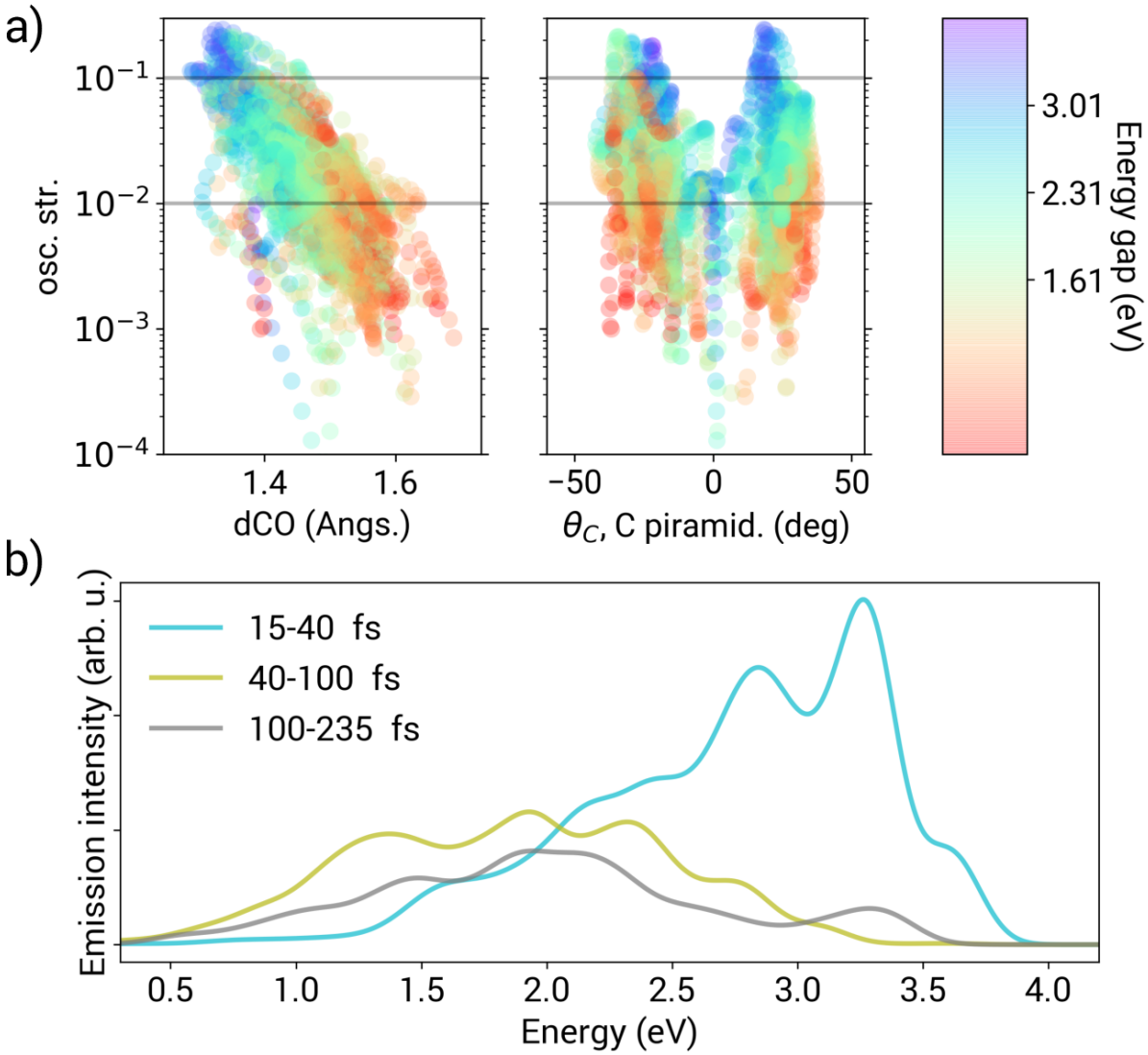

Figure 4: a) Correlation between relevant modes and oscillator strengths as obtained from nonadiabatic dynamics simulations of **2B7**. Left panel: CO stretching (Å), right panel: pyramidalization of the amide C atom (θ_C, degrees). Windows of oscillator strengths in the $10^{-2} - 10^{-1}$ range are delineated. The color scale (right) corresponds to the instantaneous S_1-S_0 energy gap. b) **2B7** emission profiles computed over three time windows and colored according to legend. The computations are performed at the ADC(2)/cc-pVDZ level.

tions play a key role in the photophysics of amyloid-like systems. This perception originates from several experimental observations and conjunctions; the hypothesis of Shukla *et al.*[49] that the intrinsic emission observed in several non aromatic protein crystals and aggregates originated from the delocalization of so-called peptide electrons over a network of intra- and intermolecular hydrogen bonds; the finding of del Mercato *et al.*[10] that the intrinsic fluorescence of amyloid-like fibrils made of poly(ValGlyGlyLeuGly) strongly depends on the presence of water molecules intercalated between β-strands; the strong reduction of fluorescence intensity observed in fully protonated or deprotonated amyloid fibrils,[12] and the deduction of Ye *et al.*[50] that the intrinsic luminescence observed in alanine, valine and isoleucine based oligopeptides arises from hydrogen bond mediated interactions between amide groups.

It is possible, although not straightforward, to establish a connection between a photophysical mechanism like this one – centered around the topography of peptides nπ^* states, and a view in which hydrogen bonding interactions are involved in the observed photophysical behavior.[12] The involvement of a carbonyl group in a hydrogen bond leads to the elongation of the C=O bond and reduces the geometrical difference between the ground state structure and the corresponding nπ^* minimum. This increases the probability of light absorption closer to the minimum of the nπ^* state and shifts the absorption toward longer wavelengths. Further, hydrogen bonding interactions facilitate the decay through fluorescence as they bestow rigidity to amyloid systems. However, they are not essential for fluorescence. The latter appears to be a rather generic property of a β-strand amide backbone and is caused by the population trapping at the minima of different nπ^* states.

With respect to previous computational studies we can observe the following; In a previous article some of us have investigated the Aβ30-35 crystal (2Y3J) and observed that in strongly hydrogen bonded N-C salt bridges the excitation energy of the corresponding nπ^* states were significantly redshifted.[12] From this trend it was assumed that electronic states localized on the termini were responsible for the fluorescence, however the fluorescence spectra were not computed and the quantitative picture was very sensitive on the employed level of theory (see Figure S7 of Ref[12]). Along the same lines, some of us studied how the chemical composition of the termini zwitterionic *vs* acetylated affects the optical properties of amyloids.[51] It was found that charge transfer states around the termini played an important role in shaping the low-energy absorption tail in the spectrum. The experimental excitation spectra exhibited the same behavior, that is reduction in the lower energy component of the excitation upon acetylation on the N-terminus. The experimental emission spectra, however, were virtually unaffected. Very recent work in collaboration with Kaminski and coworkers has shown using L-glutamine peptides, that short hydrogen bonds involving termini interactions are required to observe fluorescence.[52] With respect to the involvement of termini, in this work we have performed an ADC(2) and SCS-ADC(2) analysis of small models with deplanarized hydrogen bonded termini extracted from previous MD simulations. The results show that at the ADC(2) level the excitation energies of the nπ^* states localized on the termini are slightly red shifted, but comparable to those of inner residues (See Suporting information Sec. 2.2). However, a further reduction in excitation energies and increase in the oscillator strength is observed at the SCS-ADC(2)/aug-cc-pVDZ level. By employing model systems without hydrogen bonded termini we have shown that the necessary structural element needed to observe fluorescence is dependent on the system under study. In the case of the amyloid aggregates, this necessary structural element appears to be the cross-linked β-sheet secondary structure. Recent findings of Rosenman and co-workers that nanostructures composed of non-aromatic peptides show visible fluorescence only after they undergo transition from helical to β-sheet secondary structure fully support this view.[24]

In a series of related papers Swaminathan and co-workers[18,53,54] and Mandal *et al.*[55] have shown that in proteins rich in charged amino acid residues low-lying charge transfer excitations lead to absorption in the near UV-visible range. Unfortunately, due to the simplicity of our model systems we cannot make a connection to these results. Chen et al.[56] investigated crystals of isoleucine and proposed that clustering of non-conventional chromophores and the conformational rigidity imposed by the crystal lead to fluorescence. An excitation energy of 4.01 eV was obtained, but the emission wavelength was not computed. In the excitation under scrutiny, an electron was promoted to a Rydberg orbital (Figure S27 of Ref.[56]). We showed that the πRyd state localized on the terminal NH_2 group of **2B7** has a weak coordinate dependence. In our calculations the energy gap between the πRyd and the ground state remained above 4.2 eV, too large to account for the observed emission spectrum (see Table 2). This suggest that Rydberg states may be involved in the near UV excitation, but it is

unlikely that they are responsible for the emission in the visible part of the spectrum. Conversely, the potential energy landscape of the amide nπ^* states is not only fully compatible with the emission spectra but also with the observed Stokes shift.

More generally, the mechanism that we elucidated could also be operative in a wide range of amide-based systems showing so-called 'non-traditional' intrinsic luminescence.[57–59] These systems have interesting applications in bio-nanophotonics and we hope that the bottom-up computational approach proposed in this study will lead to an improved understanding of their photophysics.

Conclusion

The observation of visible fluorescence in non-aromatic amyloid systems has opened up very lively discussions in the literature on the underlying photophysics. In this work, we proposed a mechanism that links the optical behavior of amyloid peptides to the structural and electronic characteristics of the amide backbone. The key to understanding how amyloids absorb and emit light lies in the topography of their nπ^* states. We have shown that a localized structural deformation involving distortion of the amide or carboxyl groups with elongation of the C=O bond strongly stabilizes the corresponding nπ^* state and makes it accessible to near UV excitation. Because of the redshifted excitation and of the rigid cross β-sheet secondary structure of amyloid systems, access to CIs which typically mediate the non-radiative relaxation of peptides and proteins is reduced, forcing the system to decay through fluorescence. In very good agreement with experimental findings, we show that fluorescence takes place in the visible region of the electromagnetic spectrum. We believe that in amyloids the large number of amide groups or alternatively the large density of nπ^* states, will contribute to the possibility to observe luminescence, even in cases when only a small fraction of chromophores is excited.

The present contribution emphasizes the structural and electronic properties of the cross β-sheet secondary structure amide nπ^* states. Effects arising from H-bonded termini and the interactions between the amino acid side chains present in real amyloid systems could not be taken into account. There is little doubt that these effects are important, but serious numerical and methodological challenges prevented their accurate treatment within the framework of this study.

Computational Methods

Ground state. All ground state calculations were run using the CP2K package.[60] A convergence criterion of 5×10^{-7} a.u. was used for the optimization of the wave function. The wave function was expanded in the Gaussian double-ζ valence polarized (DZVP) basis set and an auxiliary basis set of plane waves was used up to a cutoff of 320 Ry. We employed the gradient correction to the local density approximation and Goedecker-Teter-Hutter (GTH) pseudopotentials for treating the core electrons.[61] Unless stated otherwise, all calculations employed the Becke-Lee-Yang-Parr (BLYP)[40,41] functional with the D3(0) Grimme dispersion corrections.[42] The finite temperature simulations were conducted within the canonical NVT ensemble using the canonical-sampling velocity-rescaling thermostat method.[62]

Excited states. Excited state calculations were run with Turbomole 7.0.[63] The algebraic diagrammatic construction of second order (ADC(2)) method was used for excited-state calculations.[43,44] Unless stated otherwise, the cc-pVDZ basis set was employed in all ADC(2) calculations.[64] To describe Rydberg excited states we have used the spin-component scaled version of ADC(2) (SCS-ADC(2)) and the aug-cc-pVDZ basis set.[65,66] Nonadiabatic trajectory surface hopping molecular dynamics simulations were performed employing Tully's fewest switches surface hopping algorithm.[67] A time step of 0.5 fs was used and the required nonadiabatic couplings were computed from wave function overlaps.[68,69] For further details see Supporting Information.

Supporting Information Available

Supporting Information. Specification of the model systems, theoretical methods and computational details, additional results and Cartesian coordinates of the reference **2B7(C)** structure.

Acknowledgement The authors thank W. Domcke (TUM) and N. Basarić (IRB) for helpful discussions. This research has been supported by the the Croatian Science Foundation grant HRZZ IP-2016-06-1142.

References

(1) Nelson, R.; Sawaya, M. R.; Balbirnie, M.; Madsen, A. Ø.; Riekel, C.; Grothe, R.; Eisenberg, D. Structure of the cross-β spine of amyloid-like fibrils. *Nature* **2005**, *435*, 773–778.

(2) Fitzpatrick, A. W.; Debelouchina, G. T.; Bayro, M. J.; Clare, D. K.; Caporini, M. A.; Bajaj, V. S.; Jaroniec, C. P.; Wang, L.; Ladizhansky, V.; Müller, S. A.; MacPhee, C. E.; Waudby, C. A.; Mott, H. R.; Simone, A. D.; Knowles, T. P.; Saibil, H. R.; Vendruscolo, M.; Orlova, E. V.; Griffin, R. G.; Dobson, C. M. Atomic structure and hierarchical assembly of a cross-β amyloid fibril. *Proc. Natl. Acad. Sci. U. S. A.* **2013**, *110*, 5468–73.

(3) Adamcik, J.; Mezzenga, R. Amyloid Polymorphism in the Protein Folding and Aggregation Energy Landscape. *Angew. Chem. Int. Ed.* **2018**, *57*, 8370–8382.

(4) Chiti, F.; Dobson, C. M. Protein Misfolding, Functional Amyloid, and Human Disease. *Annual Review of Biochemistry* **2006**, *75*, 333–366.

(5) Makin, O. S.; Atkins, E.; Sikorski, P.; Johansson, J.; Serpell, L. C. Molecular Basis for Amyloid Fibril Formation and Stability. *Proc. Natl. Acad. Sci. U. S. A.* **2005**, *102*, 315.

(6) Baftizadeh, F.; Biarnes, X.; Pietrucci, F.; Affinito, F.; Laio, A. Multidimensional View of Amyloid Fibril Nucleation in Atomistic Detail. *J. Am. Chem. Soc.* **2012**, *134*, 3886.

(7) Pinotsi, D.; Buell, A. K.; Galvagnion, C.; Dobson, C. M.; Kaminski Schierle, G. S.; Kaminski, C. F. Direct Observation of Heterogeneous Amyloid Fibril Growth Kinetics via Two-Color Super-Resolution Microscopy. *Nano Letters* **2014**, *14*, 339–345.

(8) Nasica Labouze, J.; Nguyen, P. H.; Sterpone, F.; Berthoumieu, O.; Buchete, N.-V.; Coté, S.; De Simone, A.; Doig, A. J.; Faller, P.; Garcia, A.; Laio, A.; Li, M. S.; Melchionna, S.; Mousseau, N.; Mu, Y.; Paravastu, A.; Pasquali, S.; Rosenman, D. J.; Strodel, B.; Tarus, B.; Viles, J. H.; Zhang, T.; Wang, C.; Derreumaux, P. Amyloid β Protein and Alzheimer's Disease: When Computer Simulations Complement Experimental Studies. *Chem. Rev.* **2015**, *115*, 3518.

(9) Cohen, S.; Cukalevski, R.; Michaels, T.; Šarić, A.; Törnquist, M.; Vendruscolo, M.; Dobson, C.; Buell, A.; Knowles, T.; Linse, S. Distinct thermodynamic signature of oligomer generation in the aggregation of the amyloid-β peptide. *Nat. Chem.* **2018**, *10*, 523–531.

(10) Del Mercato, L. L.; Pompa, P. P.; Maruccio, G.; Della Torre, A.; Sabella, S.; Tamburro, A. M.; Cingolani, R.; Rinaldi, R. Charge transport and intrinsic fluorescence in amyloid-like fibrils. *Proc. Natl. Acad. Sci. U. S. A.* **2007**, *104*, 18019.

(11) Pinotsi, D.; Buell, A. K.; Dobson, C. M.; Kaminski Schierle, G. S.; Kaminski, C. F. *ChemBioChem* **2013**, *14*, 846.

(12) Pinotsi, D.; Grisanti, L.; Mahou, P.; Gebauer, R.; Kaminski, C. F.; Hassanali, A.; Kaminski Schierle, G. S. Proton Transfer and Structure-Specific Fluorescence in Hydrogen Bond-Rich Protein Structures. *J. Am. Chem. Soc.* **2016**, *138*, 3046–3057.

(13) Pansieri, J.; Josserand, V.; Lee, S.-J.; Rongier, A.; Imbert, D.; Sallanon, M. M.; Kövari, E.; Dane, T. G.; Vendrely, C.; Chaix-Pluchery, O.; Guidetti, M.; Vollaire, J.; Fertin, A.; Usson, Y.; Rannou, P.; Coll, J.-L.; Marquette, C.; Forge, V. Ultraviolet-visible-near-infrared optical properties of amyloid fibrils shed light on amyloidogenesis. *Nat. Photonics* **2019**, *13*, 473–479.

(14) Stower, H. Searching for Alzheimer's disease therapies. *Nat. Med.* **2018**, *24*, 894–897.

(15) Johansson, P. K.; Koelsch, P. Label-free imaging of amyloids using their intrinsic linear and nonlinear optical properties. *Biomedical Optics Express* **2017**, *8*, 743.

(16) Tikhonova, T. N.; Rovnyagina, N. R.; Zherebker, A. Y.; Sluchanko, N. N.; Rubekina, A. A.; Orekhov, A. S.; Nikolaev, E. N.; Fadeev, V. V.; Uversky, V. N.; Shirshin, E. A. Dissection of the deep-blue autofluorescence changes accompanying amyloid fibrillation. *Archives of Biochemistry and Biophysics* **2018**, *651*, 13 – 20.

(17) Amdursky, N.; Molotskii, M.; Aronov, D.; Adler-Abramovich, L.; Gazit, E.; Rosenman, G. Blue Luminescence Based on Quantum Confinement at Peptide Nanotubes. *Nano Letters* **2009**, *9*, 3111–3115.

(18) Prasad, S.; Mandal, I.; Singh, S.; Paul, A.; Mandal, B.; Venkatramani, R.; Swaminathan, R. Near UV-Visible electronic absorption originating from charged amino acids in a monomeric protein. *Chemical Science* **2017**, *8*, 5416–5433.

(19) Grisanti, L.; Pinotsi, D.; Gebauer, R.; Kaminski Schierle, G. S.; Hassanali, A. A. A Computational Study on How Structure Influences the Optical Properties in Model Crystal Structures of Amyloid Fibrils. *Phys. Chem. Chem. Phys.* **2017**, *19*, 4030.

(20) Hammarström, P. Photonic amyloids. *Nat. Photonics* **2019**, *13*, 442–444.

(21) Niyangoda, C.; Miti, T.; Breydo, L.; Uversky, V.; Muschol, M. Carbonyl-based blue autofluorescence of proteins and amino acids. *PLOS ONE* **2017**, *12*, 1–15.

(22) Handelman, A.; Kuritz, N.; Natan, A.; Rosenman, G. Reconstructive Phase Transition in Ultrashort Peptide Nanostructures and Induced Visible Photoluminescence. *Langmuir* **2016**, *32*, 2847–2862.

(23) Handelman, A.; Lapshina, N.; Apter, B.; Rosenman, G. Peptide Integrated Optics. *Advanced Materials* **2018**, *30*, 1705776.

(24) Lapshina, N.; Shishkin, I. I.; Nandi, R.; Noskov, R. E.; Barhom, H.; Joseph, S.; Apter, B.; Ellenbogen, T.; Natan, A.; Ginzburg, P.; Amdursky, N.; Rosenman, G. Bioinspired Amyloid Nanodots with Visible Fluorescence. *Advanced Optical Materials* **2019**, *7*, 1801400.

(25) Serrano-Andrés, L.; Fülscher, M. P. Theoretical Study of the Electronic Spectroscopy of Peptides. 1. The Peptidic Bond: Primary, Secondary, and Tertiary Amides. *J. Am. Chem. Soc.* **1996**, *118*, 12190–12199.

(26) Serrano-Andrés, L.; Fülscher, M. P. Theoretical Study of the Electronic Spectroscopy of Peptides. 2. Glycine and N-Acetylglycine. *J. Am. Chem. Soc.* **1996**, *118*, 12200–12206.

(27) Serrano-Andrés, L.; Fülscher, M. P. Theoretical Study of the Electronic Spectroscopy of Peptides. III. Charge-Transfer Transitions in Polypeptides. *J. Am. Chem. Soc.* **1998**, *120*, 10912–10920.

(28) Chen, R. F. In *Accuracy in Spectrophotometry and Luminescence Measurements*; Mavrodineanu, R., Shultz, J. I., Menis, O., Eds.; Nat. Bureau of Standards Special Publication: Washington D.C., 1973; Vol. 378; pp 183–196.

(29) Sobolewski, A. L.; Domcke, W. Relevance of Electron-Driven Proton-Transfer Processes for the Photostability of Proteins. *ChemPhysChem* **2006**, *7*, 561–564.

(30) Shemesh, D.; Sobolewski, A. L.; Domcke, W. Efficient Excited-State Deactivation of the Gly-Phe-Ala Tripeptide via an Electron-Driven Proton-Transfer Process. *J. Am. Chem. Soc.* **2009**, *131*, 1374–1375.

(31) Shemesh, D.; Sobolewski, A. L.; Domcke, W. Role of excited-state hydrogen detachment and hydrogen-transfer processes for the excited-state deactivation of an aromatic dipeptide: N-acetyl tryptophan methyl amide. *Phys. Chem. Chem. Phys.* **2010**, *12*, 1374–1375.

(32) Mercier, S. R.; Boyarkin, O. V.; Kamariotis, A.; Guglielmi, M.; Tavernelli, I.; Cascella, M.; Rothlisberger, U.; Rizzo, T. R. Microsolvation Effects on the Excited-State Dynamics of Protonated Tryptophan. *J. Am. Chem. Soc.* **2006**, *128*, 16938–16943.

(33) Iqbal, A.; Stavros, V. G. Active Participation of $^1\pi\sigma^*$ States in the Photodissociation of Tyrosine and Its Subunits. *J. Phys. Chem. Lett.* **2010**, *1*, 2274–2278.

(34) Guglielmi, M.; Doemer, M.; Tavernelli, I.; Rothlisberger, U. Photodynamics of Lys^+-Trp protein motifs: Hydrogen bonds ensure photostability. *Faraday Discuss.* **2013**, *163*, 189.

(35) Mališ, M.; Loquais, Y.; Gloaguen, E.; Biswal, H. S.; Piuzzi, F.; Tardivel, B.; Brenner, V.; Broquier, M.; Jouvet, C.; Mons, M.; Došlić, N.; Ljubić, I. Unraveling the mechanisms of nonradiative deactivation in model peptides following photoexcitation of a phenylalanine residue. *J. Am. Chem. Soc.* **2012**, *134*, 20340–20351.

(36) Mališ, M.; Loquais, Y.; Gloaguen, E.; Jouvet, C.; Brenner, V.; Mons, M.; Ljubić, I.; Došlić, N. Non-radiative relaxation of UV photoexcited phenylalanine residues: probing the role of conical intersections by chemical substitution. *Phys. Chem. Chem. Phys.* **2014**, *16*, 2285–2288.

(37) Soorkia, S.; Jouvet, C.; Gregoire, G. UV Photoinduced Dynamics of Conformer-Resolved Aromatic Peptides . *Chem. Rev.* **2019**, *120*, 3296–3327.

(38) Crespo-Otero, R.; Li, Q.; Blancafort, L. Exploring Potential Energy Surfaces for Aggregation-Induced Emission-From Solution to Crystal. *Chem. Asian J.* **2019**, *14*, 700–714.

(39) Colletier, J.-P.; Laganowsky, A.; Landau, M.; Zhao, M.; Soriaga, A. B.; Goldschmidt, L.; Flot, D.; Cascio, D.; Sawaya, M. R.; Eisenberg, D. Molecular basis for amyloid-β polymorphism. *Proc. Nat. Acad. Sci. U.S.A.* **2011**, *108*, 16938–16943.

(40) Becke, A. D. Density-functional exchange-energy approximation with correct asymptotic behavior. *Phys. Rev. A* **1988**, *38*, 3098–3100.

(41) Lee, C.; Yang, W.; Parr, R. G. Development of the Colle-Salvetti correlation-energy formula into a functional of the electron density. *Phys. Rev. B* **1988**, *37*, 785–789.

(42) Grimme, S.; Antony, J.; Ehrlich, S.; Krieg, H. A consistent and accurate ab initio parametrization of density functional dispersion correction (DFT-D) for the 94 elements H-Pu. *J. Chem. Phys.* **2010**, *132*, 154104.

(43) Schirmer, J. Beyond the random-phase approximation: A new approximation

scheme for the polarization propagator. *Phys. Rev. A* **1982**, *26*, 2395–2416.

(44) Dreuw, A.; Wormit, M. The algebraic diagrammatic construction scheme for the polarization propagator for the calculation of excited states. *WIREs Comput. Mol. Sci.* **2015**, *5*, 82–95.

(45) Došlić, N.; Kovačević, G.; Ljubić, I. Signature of the Conformational Preferences of Small Peptides: a Theoretical Investigation. *J. Phys. Chem. A* **2007**, *111*, 8650–8658.

(46) Wallin, G.; Härd, T.; Aqvis, J. Folding-Reaction Coupling in a Self-Cleaving Protein. *J. Chem. Theory Comput.* **2012**, *8*, 3871–3879.

(47) Johansson, D. G. A.; Macao, B.; Sandberg, A.; Härd, T. SEA Domain Autoproteolysis Accelerated by Conformational Strain: Mechanistic Aspects. *J. Mol. Biol.* **2008**, *377*, 1130–1143.

(48) Lukeš, V.; Šolc, R.; Barbatti, M.; Elstner, M.; Lischka, H.; Kauffmann, H.-F. Torsional potentials and full-dimensional simulation of electronic absorption and fluorescence spectra of para-phenylene oligomers using the semiempirical self-consistent charge density-functional tight binding approach. *J. Chem. Phys.* **2008**, *129*, 164905.

(49) Shukla, A.; Mukherjee, S.; Sharma, S.; Agrawal, V.; Kishana, K. R.; Guptasarma, P. A novel UV laser-induced visible blue radiation from protein crystals and aggregates: scattering artifacts or fluorescence transitions of peptide electrons delocalized through hydrogen bonding? *Archives Biochem Biophys* **2004**, *428*, 144–153.

(50) Ye, R.; Liu, Y.; Zhang, H.; Su, H.; Zhang, Y.; Xu, L.; Hu, R.; Kwok, R. T. K.; Wong, K. S.; Lam, J. W. Y.; Goddard, W. A.; Tang, B. Z. Non-conventional fluorescent biogenic and synthetic polymers without aromatic rings. *Polym. Chem.* **2017**, *8*, 1722–1727.

(51) Jong, K. H.; Azar, Y. T.; Grisanti, L.; Stephens, A. D.; Jones, S. T. E.; Credgington, D.; Kaminski Schierle, G. S.; Hassanali, A. Low energy optical excitations as an indicator of structural changes initiated at the termini of amyloid proteins. *Phys. Chem. Chem. Phys.* **2019**, *21*, 23931–23942, and 10.26434/chemrxiv.7215065.v1.

(52) Stephens, A. D.; Qaisrani, M. N.; Ruggiero, M. T.; Jones, S. T. E.; Poli, E.; Bond, A. D.; Woodhams, P. J.; Kleist, E. M.; Grisanti, L.; Gebauer, R.; Zeitler, J. A.; Credgington, D.; Hassanali, A.; Kaminski Schierle, G. S. Intrinsic fluorescence in non-aromatic peptide structures is induced by collective vibrations, charge reorganisation and short hydrogen bonds, as shown in a new glutamine-related structure. 2020; `https://doi.org/10.1101/2020.01.22.915306`, bioRxiv.

(53) Ansari, M. Z.; Kumar, A.; Ahari, D.; Priyadarshi, A.; Lolla, P.; Bhandari, R.; Swaminathan, R. Protein charge transfer absorption spectra: an intrinsic probe to monitor structural and oligomeric transitions in proteins. *Faraday Discuss.* **2018**, *207*, 91–113.

(54) Kumar, A.; Ahari, D.; Priyadarshi, A.; Ansari, M. Z.; Swaminathan, R. Weak Intrinsic Luminescence in Monomeric Proteins Arising from Charge Recombination. *J. Phys. Chem. B* **2020**, *124*, 2731–2746.

(55) Mandal, I.; Paul, S.; Venkatramani, R. Optical backbone-sidechain charge transfer transitions in proteins sensitive to secondary structure and modifications. *Faraday Discussions* **2018**, *207*, 115–135.

(56) Chen, X.; Luo, W.; Ma, H.; Peng, Q.; Yuan, W. Z.; Zhang, Y. Prevalent intrinsic

emission from nonaromatic amino acids and poly(amino acids). *Sci. China Chem.* **2018**, *61*, 351–359.

(57) Bortolotti, A.; Wong, Y. H.; Korsholm, S. S.; Bahring, N. H. B.; Bobone, S.; Tayyab, S.; van de Weert, M.; Stella, L. On the purported "backbone fluorescence" in protein three-dimensional fluorescence spectra. *RSC Adv.* **2016**, *6*, 112870–112876.

(58) Tomalia, D. A.; Klajnert-Maculewicz, B.; Johnson, K. A.-M.; F.Brinkman, H.; Janaszewska, A.; Hedstrand, D. M. Non-traditional intrinsic luminescence: inexplicable blue fluorescence observed for dendrimers, macromolecules and small molecular structures lacking traditional/conventional luminophores. *Prog. Polym. Sci.* **2019**, *90*, 35–117.

(59) Villa, A. M.; Doglia, S. M.; Gioia, L. D.; Bertini, L.; Natalello, A. Anomalous Intrinsic Fluorescence of HCl and NaOH Aqueous Solutions. *J. Phys. Chem. Lett.* **2019**, *10*, 7230–7236.

(60) Hutter, J.; Iannuzzi, M.; Schiffmann, F.; VandeVondele, J. cp2k: atomistic simulations of condensed matter systems. *WIREs Comput. Mol. Sci.* **2014**, *4*, 15–25.

(61) Goedecker, S.; Teter, M.; Hutter, J. Separable dual-space Gaussian pseudopotentials. *Phys. Rev. B* **1996**, *54*, 1703–1710.

(62) Bussi, G.; Donadio, D.; Parrinello, M. Canonical sampling through velocity rescaling. *J. Chem. Phys.* **2007**, *126*, 014101.

(63) TURBOMOLE V7.0 2015, a development of University of Karlsruhe and Forschungszentrum Karlsruhe GmbH, 1989-2007, TURBOMOLE GmbH, since 2007; available from `http://www.turbomole.com`.

(64) Dunning, T. H. Gaussian basis sets for use in correlated molecular calculations. I. The atoms boron through neon and hydrogen. *J. Chem. Phys.* **1989**, *90*, 1007–1023.

(65) Grimme, S. Improved second-order Møller-Plesset perturbation theory by separate scaling of parallel- and antiparallel-spin pair correlation energies. *J. Chem. Phys.* **2003**, *118*, 9095–9102.

(66) Hellweg, A.; Grün, S. A.; Hättig, C. Benchmarking the performance of spin-component scaled CC2 in ground and electronically excited states. *Phys. Chem. Chem. Phys.* **2008**, *10*, 4119–4127.

(67) Tully, J. C. Molecular dynamics with electronic transitions. *J. Chem. Phys.* **1990**, *93*, 1061–1071.

(68) Hammes-Schiffer, S.; Tully, J. C. Proton transfer in solution: Molecular dynamics with quantum transitions. *J. Chem. Phys.* **1994**, *101*, 4657–4667.

(69) Sapunar, M.; Piteša, T.; Davidović, D.; Došlić, N. Highly Efficient Algorithms for CIS Type Excited State Wave Function Overlaps. *J. Chem. Theory Comput.* **2019**, *15*, 3461–3469.

Graphical TOC Entry